J|A|C|S ARTICLES

Published on Web 03/20/2009

Selective Facet Reactivity during Cation Exchange in Cadmium Sulfide Nanorods

Bryce Sadtler,[†,‡] Denis O. Demchenko,[§,∥] Haimei Zheng,[†,‡] Steven M. Hughes,[†] Maxwell G. Merkle,[†] Ulrich Dahmen,[‡] Lin-Wang Wang,[§] and A. Paul Alivisatos*[,†,‡]

Department of Chemistry, University of California, Berkeley, California 94720, and Materials Science Division and Computational Research Division, Lawrence Berkeley National Laboratory, Berkeley, California 94720

Received December 18, 2008; E-mail: alivis@berkeley.edu

Abstract: The partial transformation of ionic nanocrystals through cation exchange has been used to synthesize nanocrystal heterostructures. We demonstrate that the selectivity for cation exchange to take place at different facets of the nanocrystal plays an important role in determining the resulting morphology of the binary heterostructure. In the case of copper(I) (Cu^+) cation exchange in cadmium sulfide (CdS) nanorods, the reaction starts preferentially at the ends of the nanorods such that copper sulfide (Cu_2S) grows inward from either end. The resulting morphology is very different from the striped pattern obtained in our previous studies of silver(I) (Ag^+) exchange in CdS nanorods where nonselective nucleation of silver sulfide (Ag_2S) occurs (Robinson, R. D.; Sadtler, B.; Demchenko, D. O.; Erdonmez, C. K.; Wang, L.-W.; Alivisatos, A. P. *Science* **2007**, *317*, 355−358). From interface formation energies calculated for several models of epitaxial connections between CdS and Cu_2S or Ag_2S, we infer the relative stability of each interface during the nucleation and growth of Cu_2S or Ag_2S within the CdS nanorods. The epitaxial attachments of Cu_2S to the end facets of CdS nanorods minimize the formation energy, making these interfaces stable throughout the exchange reaction. Additionally, as the two end facets of wurtzite CdS nanorods are crystallographically nonequivalent, asymmetric heterostructures can be produced.

Introduction

The synthesis of nanocrystal heterostructures, consisting of two or more components within each particle, is important both for creating multifunctional materials and for controlling electronic coupling between nanoscale units.[2−5] As the complexity of colloidal nanocrystal heterostructures increases beyond simple spherical core−shell morphologies, their electronic structure and physical properties will strongly depend on the spatial organization of the two materials within each nanocrystal. Colloidal nanocrystals possessing anisotropic shapes provide a platform for selective chemical modification based on the relative reactivities of the different crystalline facets exposed at the surface. This enables the synthesis of multicomponent nanostructures through the nucleation and growth of a secondary material on specific facets of the nanocrystals.[4−11] While the methodology of sequential growth has been applied to a wide range of material combinations, its drawback is that the desired heterogeneous nucleation on the existing nanocrystal surface often competes with homogeneous nucleation of separate nanocrystals of the secondary material.

An alternative method for synthesizing nanocrystal heterostructures, which circumvents separate nucleation, is the transformation of a portion of the nanocrystal into a new composition or structural phase.[12−17] In ionic nanocrystals, cation exchange reactions have been used to alter the composition of the material by replacing the cations within the nanocrystal lattice with a

† Department of Chemistry, University of California.
‡ Materials Science Division, Lawrence Berkeley National Laboratory.
§ Computational Research Division, Lawrence Berkeley National Laboratory.
∥ Current address: Department of Physics, Virginia Commonwealth University, Richmond, VA 23284.

(1) Robinson, R. D.; Sadtler, B.; Demchenko, D. O.; Erdonmez, C. K.; Wang, L.-W.; Alivisatos, A. P. *Science* **2007**, *317*, 355–358.
(2) Yin, Y.; Alivisatos, A. P. *Nature* **2005**, *437*, 664–670.
(3) Jun, Y.-W.; Choi, J.-S.; Cheon, J. *Chem. Commun.* **2007**, 1203–1214.
(4) Cozzoli, P. D.; Pellegrino, T.; Manna, L. *Chem. Soc. Rev.* **2006**, *35*, 1195–1208.
(5) Casavola, M.; Buonsanti, R.; Caputo, G.; Cozzoli, P. D. *Eur. J. Inorg. Chem.* **2008**, 837–854.
(6) Shi, W.; Zeng, H.; Sahoo, Y.; Ohulchanskyy, T. Y.; Ding, Y.; Wang, Z. L.; Swihart, M.; Prasad, P. N. *Nano Lett.* **2006**, *6*, 875–881.
(7) Milliron, D. J.; Hughes, S. M.; Cui, Y.; Manna, L.; Li, J.; Wang, L.-W.; Alivisatos, A. P. *Nature* **2004**, *430*, 190–195.
(8) Mokari, T.; Rothenberg, E.; Popov, I.; Costi, R.; Banin, U. *Science* **2004**, *304*, 1787–1790.
(9) Kudera, S.; Carbone, L.; Casula, M. F.; Cingolani, R.; Falqui, A.; Snoeck, E.; Parak, W. J.; Manna, L. *Nano Lett.* **2005**, *5*, 445–449.
(10) Shieh, F.; Saunders, A. E.; Korgel, B. A. *J. Phys. Chem. B* **2005**, *109*, 8538–8542.
(11) Talapin, D. V.; Nelson, J. H.; Shevchenko, E. V.; Aloni, S.; Sadtler, B.; Alivisatos, A. P. *Nano Lett.* **2007**, *7*, 2951–2959.
(12) Sun, Y.; Xia, Y. *Science* **2002**, *298*, 2176–2179.
(13) Yin, Y.; Rioux, R. M.; Erdonmez, C. K.; Hughes, S.; Somorjai, G. A.; Alivisatos, A. P. *Science* **2004**, *304*, 711–714.
(14) Cable, R. E.; Schaak, R. E. *J. Am. Chem. Soc.* **2006**, *128*, 9588–9589.
(15) Mews, A.; Eychmuller, A.; Giersig, M.; Schooss, D.; Weller, H. *J. Phys. Chem.* **1994**, *98*, 934–941.
(16) Dloczik, L.; Koenenkamp, R. *J. Solid State Electrochem.* **2004**, *8*, 142–146.
(17) Son, D. H.; Hughes, S. M.; Yin, Y.; Alivisatos, A. P. *Science* **2004**, *306*, 1009–1012.
(18) Wark, S. E.; Hsia, C.-H.; Son, D. H. *J. Am. Chem. Soc.* **2008**, *130*, 9550–9555.

 © 2009 American Chemical Society

different metal ion.[1,15−20] For example, the addition of a small molar excess of Ag^+ cations to cadmium chalcogenide nanocrystals (CdS, CdSe, CdTe) leads to their complete conversion to the corresponding silver chalcogenide.[17] Remarkably, the shape of anisotropic nanocrystals such as rods and tetrapods is preserved after cation exchange when their dimensions are greater than the reaction zone for exchange (∼4 nm), indicating that the cohesion of the crystal is maintained during the diffusion and exchange of cations. The relative rigidity of the anion sublattice enables the partial transformation of the nanocrystal to create a heterostructure where the two compounds share a common anion. Adjusting the ratio of substitutional cations to those within the nanocrystals can be used to control the relative volume fraction of the two crystals within the binary heterostructures.[1] The spatial arrangement of materials within the nanocrystal will depend on a number of kinetic and thermodynamic factors such as the relative activation barriers for cation exchange to initiate at different facets of the nanocrystal and the energetic stability of interfaces as reaction fronts proceed through the nanocrystal. In the case of Ag^+ exchange in CdS nanorods, the reorganization of Ag_2S and CdS regions via cation diffusion causes significant changes in the morphology of the heterostructures as the fraction of Ag_2S increases within each nanorod.[1,21] Low amounts of Ag^+ produce small Ag_2S regions dotting the surface of the nanocrystals, whereas greater amounts of Ag^+ lead to alternating segments of CdS and Ag_2S along the nanorod. The large lattice strain between CdS and Ag_2S is believed to play an important role in forming the striped pattern observed for this system. Thus, it is interesting to examine a case where the lattices of the cation exchange pair have little mismatch between them.

Here we report on the synthesis of CdS−Cu_2S nanorod heterostructures synthesized by partial Cu^+ exchange. The Cu_2S regions primarily occur at one or both ends of the nanorods and appear to nucleate and grow along a single crystallographic direction. To elucidate why Cu^+ and Ag^+ cation exchange reactions with CdS nanorods produce different morphologies, models for epitaxial attachments between various facets of CdS with Cu_2S or Ag_2S lattices were used to calculate interface formation energies.[21] The formation energies indicate the favorability for interface nucleation at different facets of the nanorod and the stability of the interfaces during growth of the secondary material (Cu_2S or Ag_2S) within the CdS nanocrystal. Furthermore, the values of the interface formation energies provided by our models suggest that the asymmetric CdS−Cu_2S heterostructures observed are produced by selective Cu_2S nucleation on the $(000\bar{1})$ CdS end facet, as this interface has a lower formation energy than the attachment of Cu_2S to the opposite (0001) end.

Experimental Section

Synthesis of CdS Nanorods. Colloidal CdS nanorods were synthesized using standard techniques developed for cadmium chalcogenide nanorods.[22] The reactions were performed under air-free conditions, and the CdS nanocrystals were stored in an argon-filled glovebox. The Supporting Information provides specific reaction conditions and cleaning procedures for each batch of CdS nanorods used in this study.

Cation Exchange of CdS Nanorods. Cu^+ cation exchange was used to convert CdS nanorods into CdS−Cu_2S binary nanorods and Cu_2S nanorods. The reactions were performed inside an argon-filled glovebox at room temperature. The extent of conversion depends on the Cu^+/Cd^{2+} ratio, where an excess of Cu^+ ions (Cu^+/Cd^{2+} > 2 as two Cu^+ ions replace one Cd^{2+} ion for charge balance) leads to full conversion to Cu_2S. The molar concentration of Cd^{2+} ions for each CdS nanorod solution was determined by inductively coupled plasma atomic emission spectroscopy (ICP-AES) of acid-digested samples. Typical molar extinction coefficients for Cd^{2+} within the CdS nanorod solutions were 3×10^6 mol/cm^2 at 300 nm measured by visible absorption spectroscopy. The amount of Cd^{2+} in the CdS nanorod solution in each reaction was between 1×10^{-6} and 1×10^{-5} mol. The salt, tetrakis(acetonitrile)copper(I) hexafluorophosphate ($[MeCN]_4Cu^IPF_6$), was used in the reactions as the weak binding affinity of the anion makes the salt readily soluble in methanol such that the Cu^+ solution is miscible with the colloidal solution of nanorods dispersed in toluene. In a typical reaction, 12 mg of $[MeCN]_4Cu^IPF_6$ was dissolved in 2.5 mL of methanol (MeOH). This solution was used for full conversion or was further diluted 5- or 10-fold for partial conversion. For full conversion, the $[MeCN]_4Cu^IPF_6$ solution (∼0.6−1 mL) was added to a stirring solution of CdS nanorods in toluene (∼2 mL). For partial conversion a concentrated solution of CdS nanorods in toluene (∼50−500 μL) was added to a stirring $[MeCN]_4Cu^IPF_6$ solution (∼0.1−1 mL) diluted in toluene (∼2 mL). The color of the nanocrystal solution changes rapidly (<1 s) from yellow to golden brown after mixing of the Cu^+ and CdS solutions, and the nanorods were washed by the addition of MeOH followed by centrifugation and removal of the supernatant. To examine the effect of slow addition of Cu^+ ions, the $[MeCN]_4Cu^IPF_6$ solution was loaded into a syringe pump and added at a rate of 0.15 mL/min via a capillary needle to a stirring solution of CdS nanorods in toluene. The Supporting Information details the specific reaction conditions used to produce the CdS−Cu_2S and Cu_2S nanorods characterized in this work.

Characterization. Bright-field transmission electron microscopy (TEM) images were obtained using a Tecnai G2 S-Twin electron microscope operating at 200 kV. TEM samples were prepared by placing a drop of the nanocrystal solution onto a carbon-coated copper grid in an ambient atmosphere. The elemental distribution of the nanocrystals was characterized by energy-filtered TEM (EFTEM). The EFTEM experiments were performed using a Philips CM200 microscope or a monochromated F20 UT Technai microscope. Both microscopes were equipped with a field emission gun, an electron energy loss spectrometer, and a Gatan image filter (GIF) and were operated at 200 kV. The elemental maps were obtained by using the three-window method.[23] The Cd M-edge (404 eV) and Cu L-edge (931 eV) were used to make the color composite images. The color composites of Cd and Cu EFTEM images were made using Image-Pro Plus software. The Cu M-edge (120 eV, minor) was used for the Cu energy-filtered images.

Statistics for the length and diameter of the initial CdS nanorods and fully converted Cu_2S nanorods were gathered from bright-field TEM images using Image-Pro Plus software, and at least 150 measurements were made for each sample. Statistics for the segment lengths of the CdS and Cu_2S regions in the binary nanorods were determined from EFTEM images by making at least 150 measurements. The degree of asymmetry for each CdS−Cu_2S binary nanorod was taken to be 1 minus the ratio of the length of the short Cu_2S segment over the length of the long Cu_2S segment. Using this definition, a nanorod possessing two Cu_2S segments of equal lengths has an asymmetry value of 0, and a nanorod with Cu_2S on only one side of the nanorod has an asymmetry value of 1. The

(19) Camargo, P. H. C.; Lee, Y. H.; Jeong, U.; Zou, Z.; Xia, Y. *Langmuir* **2007**, *23*, 2985–2992.
(20) Pietryga, J. M.; Werder, D. J.; Williams, D. J.; Casson, J. L.; Schaller, R. D.; Klimov, V. I.; Hollingsworth, J. A. *J. Am. Chem. Soc.* **2008**, *130*, 4879–4885.
(21) Demchenko, D. O.; Robinson, R. D.; Sadtler, B.; Erdonmez, C. K.; Alivisatos, A. P.; Wang, L.-W. *ACS Nano* **2008**, *2*, 627–636.
(22) Peng, Z. A.; Peng, X. *J. Am. Chem. Soc.* **2002**, *124*, 3343–3353.
(23) Brydson, R. *Electron Energy Loss Spectroscopy*; BIOS Scientific: Oxford, U.K., 2001.

length fraction of the nanorod converted to Cu_2S was measured as the ratio of the combined length of Cu_2S segments over the total length of the nanorod. Thus, a nanorod that is entirely composed of CdS will have a length conversion of 0, and a nanorod fully converted to Cu_2S will have a value of 1. The CdS−Cu_2S interfaces were grouped into three categories: flat and parallel to the nanorod cross-section, flat and at an angle to the cross-section, and multifaceted (which appear curved in low-magnification TEM images). As TEM imaging provides a two-dimensional projection of the nanorod heterostructures, the apparent angle and curvature of an interface depends on its relative orientation on the TEM substrate. Therefore, the fraction of each of these types of interfaces (measured from a population of over 200 nanorods) is approximate.

The crystal structures of the samples were determined from powder X-ray diffraction (XRD) obtained on a Bruker AXS diffractometer using Co Kα radiation (1.790 Å) and a general area detector. The instrument resolution was 0.05° in 2θ, and the acquisition time for each sample was 1 h. XRD samples were prepared by dissolving the precipitated nanocrystals in a minimal amount of toluene or chloroform and using a capillary tube to drop the solution onto a glass sample plate.

Ab Initio Calculations. Supercell geometries for CdS−Cu_2S epitaxial attachments were studied using the Vienna ab initio simulation package (VASP), a density functional theory (DFT) code using planewaves and pseudopotentials.[24,25] The generalized gradient approximation (GGA) was used for the exchange-correlation part, along with projector-augmented wave (PAW) pseudopotentials and planewave energy cutoffs of 280 eV. We used Γ-point-only eigenenergies in the Brillouin zone as the supercells are sufficiently large to ensure weak dispersion of energy bands. All geometries were relaxed to have the forces on atoms reduced to 0.01 eV/Å or less. The lattice parameters of the relaxed cells were used in all calculations, and a comparison of these to the experimentally measured values is provided in the Supporting Information. CdS−Cu_2S interface formation energies for epitaxial attachments between different facets of the two crystals were computed analogously to our previous calculations for the CdS−Ag_2S system where the interface formation energy is defined as the ab initio total energy difference of the supercell containing the interface and its bulk constituents.[21] Total formation energies containing both chemical and elastic contributions were obtained by using the difference in energy between the supercell and natural bulk structures. To calculate the chemical energy alone, the bulk lattices were strained similarly to the lattice in the supercell. The elastic contributions were computed assuming the distortions occurred in the Cu_2S or Ag_2S cell only to match to the lattice of the CdS cell. The cell thicknesses for Cu_2S were 13.5 Å for the end-on and angled attachments to CdS and 27.3 Å for the side attachment. CdS−Ag_2S interface formation energies for similar end-on connections to the CdS nanorods were previously calculated,[21] and an additional side attachment was modeled for this work. The cell thicknesses for Ag_2S were 13.7 Å in all cases.

Results

Structural Characterization of CdS−Cu_2S Binary Nanorods. XRD patterns of the CdS nanorods before and after the addition of increasing amounts of Cu^+ cations are shown in Figure 1. The addition of excess Cu^+ cations relative to the amount of Cd^{2+} within the wurtzite CdS nanocrystals leads to their complete transformation to the low-temperature form of chalcocite Cu_2S as measured from XRD patterns of the reactant and product nanorods (Figure 1 and Supporting Information Figure 1).[26] Partially converted samples made by substoichiometric addition of Cu^+ ions show a combination of diffraction peaks from both CdS and Cu_2S. Peaks belonging to the CdS phase disappear and peaks belonging to Cu_2S grow stronger in intensity with increasing amounts of Cu^+ added to the solution of CdS nanorods. The bright-field transmission TEM images in Figure 2 show that, after complete Cu^+ cation exchange, the shape and size of the nanorods is preserved within the 8% contraction in lattice volume upon conversion from CdS to Cu_2S.

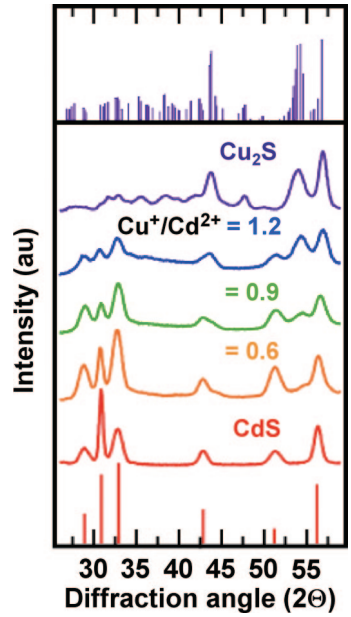

Figure 1. XRD patterns of initial CdS nanorods (bottom, red) and CdS−Cu_2S binary nanorods formed with increasing amounts of Cu^+. The addition of excess Cu^+ cations leads to full conversion of the wurtzite nanorods into the low-temperature phase of chalcocite Cu_2S. The Cu^+/Cd^{2+} cation ratio used for the partial exchange reactions is provided above each plot. Patterns from the Joint Committee on Powder Diffraction Standards (JCPDS) for wurtzite CdS (bottom, JCPDS no. 00-041-1049, space group *P*63*mc* (No. 186)) and low-temperature chalcocite Cu_2S (top, JCPDS no. 00-033-0490, space group *P*21/*c* (No. 14)) are included for reference.

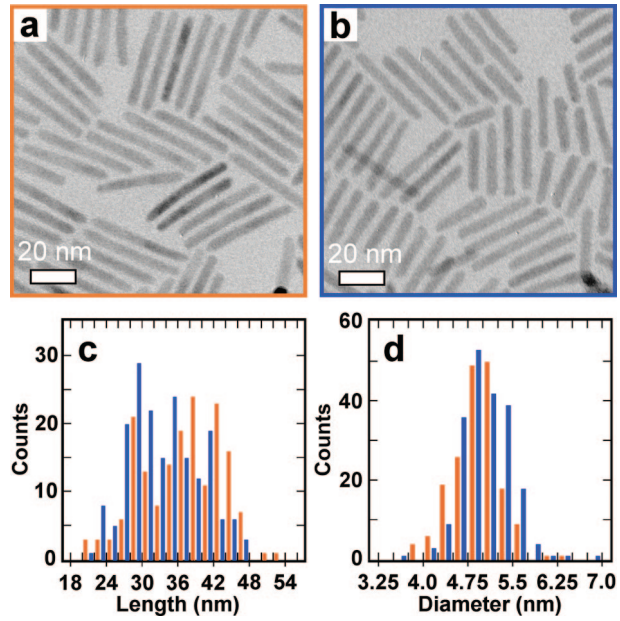

Figure 2. TEM images of (a) the initial CdS nanorods and (b) Cu_2S nanorods after complete Cu^+ exchange, showing shape preservation of the nanorods. (c) Length distributions of the nanorods before (orange) and after (blue) cation exchange. (d) Diameter distributions of the nanorods.

(24) Kresse, G.; Furthmuller, J. *Comput. Mater. Sci.* **1996**, *6*, 15–50.
(25) Kresse, G.; Furthmuller, J. *Phys. Rev. B* **1996**, *54*, 11169–11186.
(26) Evans, H. T. *Nat. Phys. Sci.* **1971**, *232*, 69–70.

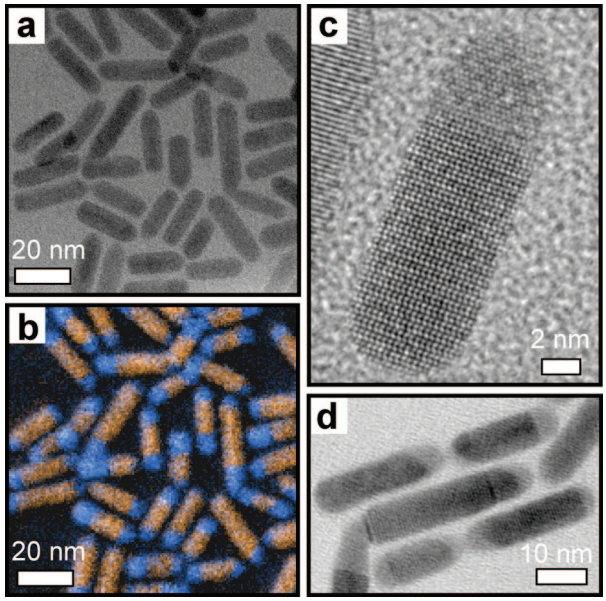

Figure 3. TEM images of CdS−Cu_2S binary nanorods: (a) bright-field (zero-loss) image, (b) color-composite EFTEM image, where the orange regions correspond to the Cd energy-filtered mapping and blue regions correspond to the Cu mapping, (c) high-resolution TEM image of a CdS−Cu_2S nanorod, (d) bright-field TEM image, where CdS−Cu_2S interfaces can be seen at various angles relative to the nanorod cross-section.

For partial Cu^+ exchange, EFTEM was used to obtain elemental mappings of the Cu- and Cd-containing regions of the binary nanorods. The composite energy-filtered image in Figure 3 clearly shows the CdS and Cu_2S portions of the binary nanorods, where the ends of the nanorods have been converted to Cu_2S (see Supporting Information Figure 2 for the original Cd and Cu EFTEM images used to make the color composite). The preferential conversion of the ends of the nanorods occurs for varying lengths, diameters, and aspect ratios. Observing nanorods with different fractions of conversion to Cu_2S, the EFTEM images indicate that cation exchange starts at the ends, and the Cu_2S regions grow into the nanorods upon further exchange. The only cases where Cu_2S segments existed between regions of CdS were at sites of irregularities such as kinks along the nanorod diameter or at the zinc-blende branch point of bipod and tripod nanocrystals.[27]

The high-resolution TEM (HRTEM) image of a Cu_2S−CdS heterostructure in Figure 3c shows the epitaxial interface between the two materials within the nanorod.[28] The majority of interfaces are flat and parallel to the cross-section of the nanorod (parallel to the (0001) plane of CdS). However, a significant population of interfaces (up to 30% in various samples) are at an angle of up to ∼40° relative to the nanorod cross-section (see Figure 3d). As the apparent angle of the interface depends on the relative orientation of the nanorod on the TEM substrate, it is likely that these interfaces occur along specific crystallographic facets of the two lattices, rather than at a continuous range of angles. Some interfaces observed by HRTEM consist of multiple facets and appear curved at lower magnifications. Step edges were also observed in some interfaces, which naturally arise if only a portion of cations within an atomic layer is exchanged.

While Cu^+ cation exchange occurs at both ends of the CdS nanorods, the relative lengths of the two Cu_2S end segments within a given nanorod can vary significantly. As the CdS wurtzite lattice lacks inversion symmetry about the *c* axis, the (0001) and $(000\bar{1})$ end facets of the nanorods are crystallographically nonequivalent.[27] Cd atoms at a $(000\bar{1})$ surface facet expose three dangling bonds, whereas Cd atoms at a (0001) surface expose only one dangling bond. Thus, the bonding arrangement of Cd atoms to the interfacial sulfur layer at the CdS−Cu_2S attachment will be different at opposite ends of the nanorod. Two important factors found to affect the asymmetry of the Cu_2S end segments are the shape (curvature and diameter) of the ends of the CdS nanorods and the rate of addition of the Cu^+ ions to the CdS solution.

Figure 4 shows Cu EFTEM images for three CdS−Cu_2S binary nanorod samples along with histograms of the asymmetry of the length of the Cu_2S segments within individual nanorods for each of the samples shown. To examine the effect of the nanocrystal dimensions on the asymmetry of Cu_2S segments, partial Cu^+ exchange was performed on nanorods of different lengths and diameters. Sample 1 shown in Figure 4a used CdS nanorods with an average length of 48 ± 7 nm (average ± first standard deviation) and a diameter of 6 ± 0.8 nm. The molar ratio of Cu^+ cations relative to Cd^{2+} was 0.51. In this case, the Cu_2S segment lengths are symmetric, evident by the continual decrease in counts in the asymmetry histogram in Figure 4d from 0 to 1. The mean asymmetry for this sample was 0.25, where the asymmetry of the two Cu_2S segments in a given binary nanorod is defined as 1 minus the ratio of the length of the short segment length over the length of the long segment. In sample 2 shown in Figure 4b, a Cu^+/Cd^{2+} ratio of 0.56 was used to make CdS−Cu_2S heterostructures from CdS nanorods with a smaller average length but larger diameter (length 29 ± 4 and diameter 9 ± 0.8 nm). The reaction produced asymmetric heterostructures, as the counts in the asymmetry histogram tend to increase from 0 to 1 (mean asymmetry 0.6). As seen in Figure 4, a significant difference between the two nanorod samples is that the ends of smaller diameter nanorods in sample 1 possess higher curvature (indicating they are composed of multiple surface facets). This appears to lead to a higher fraction of curved (multifaceted) interfaces in sample 1 (∼18%) compared to sample 2 (∼2%). On the other hand, there appears to be no correlation between the asymmetry of the Cu_2S segments and the length of the nanorods.

Sample 3 used the same initial nanorods as sample 2, but the Cu^+ solution was added dropwise via a syringe pump to the CdS solution. Slowing the rate of addition of Cu^+ cations to the CdS nanorods has several significant effects on the morphology of the CdS−Cu_2S heterostructures. First, it greatly enhances the asymmetry of the heterostructures, leading to a majority of nanorods with Cu_2S only on one end as shown in Figure 4c (sample 3, mean asymmetry 0.91). It also widens the distribution of the fraction exchanged among the individual nanorods within sample 3 (see Figure 4e). Thus, the disparity of Cu_2S segment sizes both within individual nanorods and among the different nanorods in a sample increases from sample 1 to sample 2 to sample 3. Finally, sample 3 has fewer nanorods with interfaces that are at an angle to the cross-section of the nanorod (∼15% for sample 3 versus ∼30% for sample 2). Thus, the slow addition of Cu^+ cations appears to increase the

(27) Manna, L.; Scher, E. C.; Alivisatos, A. P. *J. Am. Chem. Soc.* **2000**, *122*, 12700–12706.
(28) We observe electron beam induced changes to the Cu_2S crystal structure similar to previous reports in Cu_2S thin films,[41] which prevent analysis of the CdS−Cu_2S nanorod structure by HRTEM.

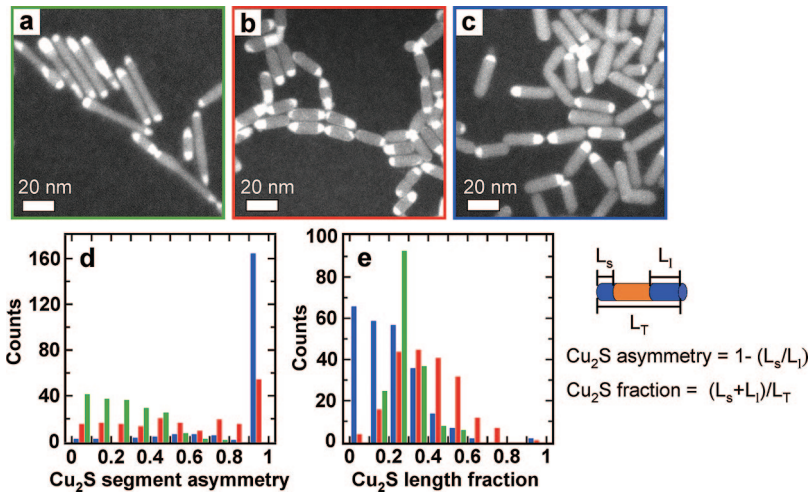

Figure 4. Cu EFTEM images of CdS−Cu_2S binary nanorods and corresponding size statistics of the Cu_2S and CdS regions. The bright regions in the images correspond to Cu_2S and the gray regions to the CdS portions of the nanorods. The green, red, and blue bars in the histograms correspond to samples 1, 2, and 3 shown in (a), (b), and (c), respectively. The three samples were made under the following conditions: (a) sample 1, initial CdS nanorods with dimensions of 48 × 6 nm and fast addition to the Cu^+ solution; (b) sample 2, CdS nanorods with dimensions of 29 × 9 nm and fast addition to the Cu^+ solution; (c) sample 3, the same initial nanorods as sample 2, but with slow addition of Cu^+ ions. (d) Histograms of the asymmetry of the Cu_2S segment lengths on the ends of the nanorods for the three samples. (e) Histograms of the Cu_2S length fraction within the binary nanorods. The asymmetry and length fraction of the Cu_2S segments are defined to the right.

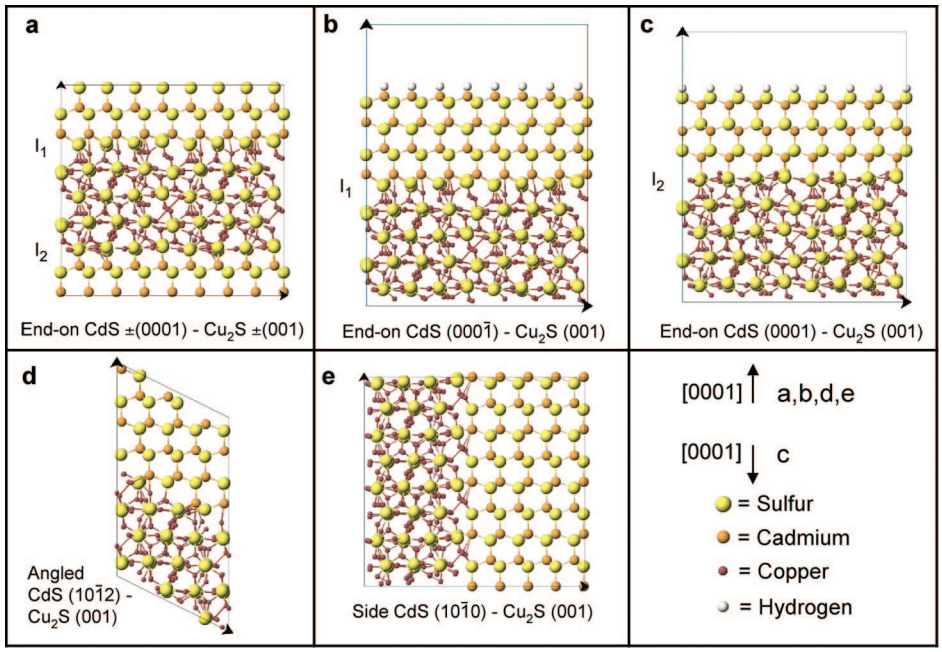

Figure 5. Models of the CdS−Cu_2S epitaxial attachments corresponding to the interface formation energies listed in Table 1. Two-dimensional projections of the lattices are shown for clarity. (a) End-on, CdS−Cu_2S attachment using the Cu_2S orthorhombic cell. This supercell contains two nonequivalent interfaces labeled as I_1 and I_2. (b) Supercell containing I_1 only connecting Cu_2S to the (000$\bar{1}$) CdS facet and (c) supercell containing I_2 connecting Cu_2S to the (0001) facet of CdS. These two supercells also possess CdS and Cu_2S surfaces, which are subtracted out to separate the formation energies for I_1 and I_2. (d) Angled, CdS−Cu_2S interface formed with the original monoclinic Cu_2S lattice connecting to hexagonal CdS. (e) Side, CdS−Cu_2S interface connecting orthorhombic Cu_2S to the (10$\bar{1}$0) facet of the CdS nanorod.

selectivity for nucleation of one CdS−Cu_2S interface per nanorod that is parallel to the nanorod cross-section.

Modeling of the CdS−Cu_2S Epitaxial Attachment. The nucleation and growth of Cu_2S within a CdS nanocrystal involves complex atomic motions, making the microscopic mechanism for this solid-state reaction relatively difficult to model. However, the formation energies for CdS−Cu_2S interfaces created at different facets of the CdS crystal give a measure of their relative stability, where interfaces with low formation energies should be observed more frequently. We constructed models of epitaxial connections between different facets of wurtzite CdS and chalcocite Cu_2S shown in Figure 5, which were used to calculate interface formation energies, defined as the total energy difference of the supercell containing the interface and its bulk constituents. The values are presented in Table 1, along with interface formation energies for CdS−Ag_2S attachments previously calculated using the same method.[21] Table 1 includes both chemical formation energies, reflecting the strength of interfacial Cd−S−Cu (Cd−S−Ag) bonds, and the elastic contribution due to lattice distortions from the

Table 1. Interface Formation Energies (eV per Interface Unit Containing One S Atom) for Attachments of CdS to Cu_2S or Ag_2S[a]

	end-on CdS ±(0001)[b] to orthorhombic Cu_2S ±(001) $(I_1 + I_2)/2$	end-on CdS (000$\bar{1}$) to orthorhombic Cu_2S (001) (I_1 only)	end-on CdS (0001) to orthorhombic Cu_2S (001) (I_2 only)	angled CdS ±(10$\bar{1}$2) to monoclinic Cu_2S ±(001)	side CdS ±(10$\bar{1}$0) to orthorhombic Cu_2S ±(001)	end-on CdS ±(0001) to orthorhombic Ag_2S ±(001)[c]	end-on CdS ±(0001) to orthorhombic Ag_2S ±(100)[c]	side CdS ±(10$\bar{1}$0) to orthorhombic Ag_2S ±(001)
chemical	0.204	0.116	0.292	0.348	0.83	−0.3	−0.87	−1.15
chemical + elastic	0.255	0.161	0.349	0.416	0.85	1.51	1.57	2.81

[a] The lattices and facets comprising each interface are listed. The chemical contribution to the formation energy and the sum of the chemical and elastic contributions are provided for each interface. The elastic contributions were computed assuming the distortions occurred in Cu_2S or Ag_2S only to match the lattice of CdS. The thicknesses of the Cu_2S cells were 13.5 Å for the end-on and angled attachments and 27.3 Å for the side attachment. The Ag_2S thicknesses were 13.7 Å in all cases. [b] The ± symbol indicates that facets with opposite (*hkl*) or (*hkil*) indexes comprise the two interfaces in the supercell. [c] Values calculated in ref 21. The end-on CdS−Ag_2S formation energies were not separated into connections to the (0001) and (000$\bar{1}$) CdS facets as the Ag_2S segments were observed to be uniform in size.[1] Thus, the reported values are an average of the two CdS−Ag_2S interfaces comprising the supercell.

epitaxial mismatch. While the value of the interfacial strain energy depends on the thickness of the Cu_2S (Ag_2S) cells used in the calculation, a comparison of the elastic contributions is useful, as strain has been shown to play an important role in forming the striped pattern observed in CdS−Ag_2S heterostructures produced by Ag^+ cation exchange.[1,21]

As the hexagonal close-packed (hcp) sulfur sublattices in CdS and Cu_2S are crystallographically nearly identical,[29] epitaxial attachments can be made by aligning the sulfur lattices of the two crystals. While the unit cell of low chalcocite is monoclinic, it is common to model it as pseudo-orthorhombic, making the symmetry of the lattice easier to visualize (see Supporting Information Figure 3).[26,30] To align the *c* axes of the hcp sulfur lattices, the [001] axis of the orthorhombic Cu_2S cell is made parallel with the [0001] axis of the hexagonal CdS lattice. The attachment of orthorhombic Cu_2S to the (000$\bar{1}$) and (0001) end facets of CdS naturally creates interfaces parallel to the cross-section of the nanorod as shown in Figure 5a. However, because the CdS lattice lacks inversion symmetry about the *c* axis, these two interfaces have different epitaxies, which are labeled as I_1 and I_2. In the interface I_1, connecting Cu_2S to the (000$\bar{1}$) CdS facet, each Cd atom bonds to three S atoms in the interfacial layer, while in the interface I_2, connecting Cu_2S to the (0001) CdS facet, each Cd atom has one bond to an interfacial S atom.

The supercell geometry used to calculate the interface formation energies implies infinite repetition of alternating CdS and Cu_2S slabs, such that two interfaces are always present. In the case of the supercell in Figure 5a, where the bonding arrangements of Cd atoms in the interfacial layer significantly differ for the two attachments, it is necessary to separate their formation energies. The detailed procedure for determining the individual energies of these two interfaces is provided in the Supporting Information. Briefly, we construct the supercells shown in Figure 5b,c, which include a single CdS−Cu_2S interface (I_1 or I_2) and the opposite CdS and Cu_2S surfaces separated by a vacuum. The supercell in Figure 5b contains the interface I_1, along with a Cd-terminated (0001) CdS surface passivated with pseudo-hydrogen atoms[31] and an unpassivated (00$\bar{1}$) Cu_2S surface. The supercell in Figure 5c contains the interface I_2, along with a S-terminated (000$\bar{1}$) CdS surface passivated with pseudo-hydrogen atoms and the same unpassivated (00$\bar{1}$) Cu_2S surface as in Figure 5b. To determine the individual energies for I_1 and I_2, the CdS and Cu_2S surface energies in each supercell as well as the difference in the number of Cu and Cd atoms between the two supercells must be taken into account. The nonequivalent CdS surface energies are subtracted out from each of the two supercells using auxiliary CdS constructions (shown in Supporting Information Figure 5).[32] The difference in the number of atoms in the two supercells is accounted for by incorporating the chemical potentials of individual Cu and Cd atoms into the bulk chemical potential of the lattices. The remaining Cu_2S surface energies cancel out by taking the difference between the formation energies of the two supercells, leaving only the energy difference between I_1 and I_2.[33] Combining the energy difference between the two interfaces with their average determined from the supercell in Figure 5a leads to the desired individual formation energies for Cu_2S attached to the wurtzite CdS (0001) or (000$\bar{1}$) facets. As seen in Table 1, the interface I_1 has a chemical formation energy that is about 2.5 times lower than that of I_2.

Due to the small lattice mismatch between the sulfur lattices of CdS and Cu_2S, the formation energies are determined primarily by the distributions of Cu and Cd atoms at the interface. The optimal geometry for metal atoms bonded to the interfacial layer of sulfur atoms should satisfy local electron counting rules; i.e., each S atom should have a local environment that supplies two electrons to fill the sulfur 3p bands (see the Supporting Information for further details). While the Cu atoms are somewhat disordered in the interfaces I_1 and I_2, it can be seen that they form layers parallel to the interface, making it relatively easy to move Cu atoms from one layer to another. By moving four Cu atoms from the Cu layer at interface I_1 to that of I_2, local electron counting is satisfied. However, this is not true for the other CdS−Cu_2S epitaxial connections that we modeled. Due to the relative orientation of the Cu atomic layers to the interface in the models described below, we were not able to satisfy local electron counting rules, which contributes to their higher formation energies.

Using the original monoclinic lattice for chalcocite Cu_2S, the sulfur lattices can be matched by connecting the ±(001) facets of Cu_2S to the ±(10$\bar{1}$2) facets of CdS. This interface appears at an angle of ∼35° to the nanorod cross-section when viewed along the [100] direction of the Cu_2S lattice, and the apparent angle of the interface will vary with its orientation on the TEM

(29) Cook, W. R., Jr.; Shiozawa, L.; Augustine, F. *J. Appl. Phys.* **1970**, *41*, 3058–3063.
(30) Sands, T. D.; Washburn, J.; Gronsky, R. *Physica Status Solidi A* **1982**, *72*, 551–559.
(31) Wang, L. W.; Li, J. *Phys. Rev. B* **2004**, *69*, 153302−1–4.
(32) Zhang, S. B.; Wei, S.-H. *Phys. Rev. Lett.* **2004**, *92*, 086102−1−4.
(33) To cancel out the Cu_2S surface energies, both the supercells in Figure 5b,c connect the (001) facet of Cu_2S to CdS such that the same (00$\bar{1}$) Cu_2S surface is exposed for both supercells. Thus, the interface I_2 in Figure 5c is different from that in Figure 5a, which connects the (00$\bar{1}$) facet of Cu_2S to CdS. However, as both I_2 connections to the (0001) CdS facet exhibit a similar bonding arrangement of interfacial Cu atoms, their formation energies should be similar.

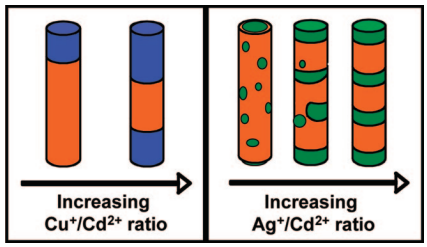

Figure 6. Development of the morphology of binary nanorods produced by cation exchange for increasing amounts of Cu^+ or Ag^+ added to CdS nanorods.

substrate.[34] Not only does the hexagonal-monoclinic interface have a larger formation energy than I_1 and I_2, but it also produces a greater total interfacial area. Only a minority of the interfaces observed were at an angle to the nanorod cross-section (<30% for fast addition and <15% for slow addition of Cu^+). We also modeled the attachment of orthorhombic Cu_2S to the $\pm(10\bar{1}0)$ side facets of the CdS nanorod as shown in Figure 5e.[35] This interface has a significantly greater formation energy than the other three connections, and Cu_2S regions were rarely observed on the sides of the nanorods. This is unlike Ag^+ exchange of CdS nanorods, where small Ag_2S regions form on both the sides and ends of the CdS nanorods in the initial stages of the reaction.

As seen in Table 1, there are several notable distinctions between the formation energies of the modeled CdS−Cu_2S and CdS−Ag_2S interfaces. First, while the chemical contributions for each of the CdS−Cu_2S formation energies are positive, they are negative for each of the CdS−Ag_2S interfaces.[36] Second, the elastic contributions are much smaller for all of the CdS−Cu_2S interfaces compared to the CdS−Ag_2S interfaces due to the smaller mismatch between the CdS and Cu_2S lattices. Furthermore, there is a larger energetic difference between the elastic contributions of the side and end-on CdS−Ag_2S connections compared to the CdS−Cu_2S connections. The importance of these differences in the development of the heterostructure morphology during cation exchange is discussed below.

Discussion

Comparison of Cu^+ and Ag^+ Cation Exchange. The heterostructure morphologies for different conversion fractions of the CdS nanorods to Cu_2S or Ag_2S aid in elucidating the movement of the reaction fronts during cation exchange within the nanocrystals.[21] Figure 6 provides a general schematic of the changes in morphology of the CdS−Cu_2S and CdS−Ag_2S binary nanorods as the Cu^+/Cd^{2+} or Ag^+/Cd^{2+} ratio increases (for partial exchange the cation ratio is between 0 and 2). First, a major difference between the two systems is that the Cu_2S segments are found primarily at the ends of the CdS nanorods at all stages of the exchange reaction, whereas the Ag_2S regions begin randomly distributed and become fewer in number as they grow into the nanorod. Second, while the multiple Ag_2S segments within a CdS nanorod are relatively uniform in size once they span the diameter of the nanorod,[1] the two Cu_2S segments can have significantly different lengths. We rationalize the observed differences in morphology through the values of the chemical and elastic contributions to the CdS−Cu_2S and CdS−Ag_2S interface formation energies listed in Table 1.

In the CdS−Cu_2S system, where the elastic contributions to the interface formation energies are small, the relative values of the chemical formation energies determine the stability of the different CdS−Cu_2S attachments. The end-on Cu_2S attachments, parallel to the nanorod cross-section, possess the lowest chemical formation energies and are the interfaces observed most often by TEM in the heterostructures. The angled attachment connecting the basal facets of the monoclinic Cu_2S lattice to CdS both has a higher chemical formation energy per interfacial unit and produces a greater interfacial area. Correspondingly, angled interfaces occur at a significantly lower frequency, particularly in the case where the Cu^+ ions are slowly added to the CdS solution. Finally, growth of Cu_2S on the sides of the CdS nanorods is rarely observed, which correlates with the calculated chemical formation energy that is approximately 7 times greater than that of end-on connection to the $(000\bar{1})$ CdS facet. The initial nucleation of CdS−Cu_2S interfaces at the ends of the nanorods is a low-energy configuration that is maintained as the exchange front moves along the length of the nanorod. Thus, the basic morphology of the nanorods possessing Cu_2S segments at one or both ends is the same for different conversion fractions. As discussed in the next section, the asymmetry of Cu_2S segment lengths is attributed to the difference in chemical formation energies for the connection of Cu_2S to opposite ends of the nanorods.

We have previously reported that when relatively low amounts of Ag^+ are added to CdS nanorods ($Ag^+/Cd^{2+} < 0.5$), small Ag_2S regions are found dispersed randomly over the surface of the nanocrystals.[1,21] At higher conversion fractions of Ag^+ exchange ($0.5 < Ag^+/Cd^{2+} < 0.9$), the Ag_2S regions coalesce such that they form segments that span the diameter of the nanorod and possess flat interfaces parallel to the nanorod cross-section. The negative chemical formation energies for each of the CdS−Ag_2S attachments favor the creation of Cd−S−Ag interfacial bonds on both the ends and sides of the CdS nanorods, leading to nonselective nucleation. However, as the Ag_2S regions grow into the nanorods, the elastic strain becomes a more important contribution to the total formation energy, driving ripening of the Ag_2S regions to reduce the interfacial area. When the Ag_2S regions grow to span the diameter of the nanorod, the interfaces parallel to the length of the nanorod disappear, which possess the greatest elastic energy (see Table 1). At this point the ripening process becomes kinetically hindered, as further exchange of cations between the flat interfaces of the Ag_2S and CdS segments would increase the interfacial area until two like segments fully merge. While full phase segregation of the CdS and Ag_2S regions to opposite ends of the nanorod would produce the lowest energy structure, the Ag_2S segments are stabilized by the large interfacial strain, leading to a repulsive elastic interaction between like segments that decreases with increasing separation between them.[1,21] Both the size and the spacing of the Ag_2S segments tend to be uniform as this minimizes the repulsive elastic interaction. Thus, nonselective nucleation followed by partial phase segregation leads to a metastable configuration consisting of alternating CdS

(34) As the distortions occur primarily in the Cu_2S lattice, we define the angle of this interface by the angle between the CdS $(10\bar{1}2)$ and (0001) planes.

(35) The supercell shown in Figure 5e has been extended along the CdS [1000] direction and shortened along the $[10\bar{1}0]$ direction for clarity. The original supercell is shown in Supporting Information Figure 4.

(36) This difference can be partially understood by comparing the bonding character and atomic structure in Cu_2S and Ag_2S. We found that the Cu−S bonds exhibit more ionic character compared to Ag−S bonds, resulting in weaker bonding at the interface and therefore a higher formation energy. Furthermore, while the positions of Ag atoms at the CdS−Ag_2S interface are close to the optimal bulk positions, relatively large rearrangements of Cu atoms are needed for them to connect to the interfacial sulfur layer. Such rearrangements increase the formation energy of the CdS−Cu_2S interface.

and Ag_2S segments. This is very different from the CdS−Cu_2S case, where, once the Cu_2S regions nucleate at the ends of the nanorods, they grow until they meet in the middle.

Asymmetry of Cu^+ Cation Exchange. The relative activation barriers for nucleation at each end of the nanorod control the asymmetry of the Cu_2S segments. In principle, disparate rates of diffusion of cations in opposite directions along the nanorod could also contribute to asymmetric growth. However, previous kinetic studies of cation exchange suggest that interface nucleation provides the main kinetic barrier for transformation of the nanocrystal.[37] The chemical formation energy for the Cu_2S attachment to the CdS $(000\bar{1})$ facet (I_1) is lower by ∼0.18 eV per Cd−Cu−S unit compared to attachment to the (0001) facet (I_2). Moreover, the $(000\bar{1})$ end facet of the CdS nanocrystal is believed to be the least stable surface of the nanorod as Cd termination leads to three dangling bonds per atom, making full passivation difficult without significant surface reconstruction.[38] Therefore, the connection of orthorhombic Cu_2S to the $(000\bar{1})$ end of the nanorods produces the thermodynamically most stable configuration as it both removes a high-energy surface and creates the lowest energy interface. This suggests that asymmetric CdS−Cu_2S nanorods are produced by selective nucleation of Cu_2S at the $(000\bar{1})$ end of the nanorod.

The increased asymmetry of Cu_2S segments in sample 2 over sample 1 as shown in Figure 4 is attributed to the larger diameter and flatter ends of the initial CdS nanorods used to produce sample 2. The shape of the CdS nanorods is kinetically determined during their growth by the relative rates of monomer addition along different crystallographic directions of the particle.[27,39] Under the nonequilibrium growth conditions used to produce highly anisotropic nanocrystals, the $(000\bar{1})$ and (0001) ends of the nanorods are partially replaced by the more stable $\{10\bar{1}1\}$-type facets, leading to pencil- or arrow-shaped nanorods.[27] The epitaxy of the nucleating interface during cation exchange will depend on the surface area of the different crystalline facets exposed. The binary nanorods in sample 1 (Figure 4a) in which the initial nanorod ends have a higher curvature compared to those used to make sample 2 (Figure 4b) also have a higher fraction of curved interfaces. Nanorods with multifaceted (curved) end faces expose less of the (0001) and $(000\bar{1})$ surfaces, which may lower the selectivity for interface nucleation at one end. Furthermore, a larger diameter will accentuate the difference in total formation energy between I_1 and I_2. As larger diameter nanorods generally also possess flatter ends, these two parameters act in concert to increase the asymmetry of the Cu_2S segment lengths.

Maintaining a low concentration of Cu^+ ions present in solution during the exchange reaction enhances the formation of a single interface in each binary nanorod. This can be seen as the asymmetry of Cu_2S segments greatly increases for slow (sample 3, Figure 4c) versus fast (sample 2, Figure 4b) addition of Cu^+ cations to the same initial batch of CdS nanorods. In addition, the percentage of interfaces at an angle to the nanorod cross-section decreases for slow addition. However, the distribution of the fraction converted to Cu_2S among individual nanorods widens, indicating that nucleation and growth of Cu_2S become increasingly overlapped in time. This is expected as the concentration of Cu^+ cations during the early stages of the dropwise addition is not enough for nucleation to occur on all of the nanorods at once. Previous studies on the reaction kinetics of Ag^+ cation exchange in CdSe nanocrystals support a mechanism where, once an interface nucleates in a nanocrystal by cation exchange at the surface, the kinetic barrier for further exchange is relatively low.[37] Thus, upon slow addition of Cu^+ ions, exchange will occur more rapidly at CdS−Cu_2S interfaces that have already formed over the creation of new interfaces, widening the distribution of the Cu_2S fraction among the nanorods. The temporal separation of nucleation and growth stages is often used to achieve monodisperse colloidal nanostructures.[22,40] In the present case we have attempted only rapid addition of the CdS and Cu^+ solutions or slow injection of Cu^+ at a constant rate. With further optimization of the rate of Cu^+ addition throughout the course of the reaction it may be possible to maximize the selectivity for nucleation on the $(000\bar{1})$ facet while also separating the nucleation and growth stages to yield a narrow distribution of Cu_2S within the nanorods.

Conclusions

We have demonstrated that the crystallographic selectivity for cation exchange to occur at different facets of ionic nanocrystals plays a critical role in determining the morphology of the resulting nanocrystal heterostructures. The preferential nucleation and growth of Cu_2S at the ends of CdS nanorods during Cu^+ exchange is attributed to the high stability of CdS−Cu_2S interfaces formed at these facets. In comparison, nonselective nucleation in Ag^+ exchange leads to the formation of multiple Ag_2S regions within the nanorod. The differences between these two systems lie in both the chemical favorability for creating interfacial bonds and the elastic distortions between attachments connecting various facets of the two materials. The relative stabilities of the interfaces we have modeled correlate well with the frequency that the corresponding morphologies are observed. In the future, similar modeling of the epitaxy in nanoscale heterostructures may be applied to other material pairs to predict which interfaces will be the most stable. As both the shape and size of the nanocrystals determine the crystallographic facets exposed at the surface, these parameters can be used to control the nanocrystal's reactivity. Selective facet reactivity can in turn provide tunability of the physical properties of nanocrystal heterostructures through control of the spatial arrangement of their components.

Acknowledgment. This work was supported by the Director, Office of Science, Office of Basic Energy Sciences, of the U.S. Department of Energy under Contract No. DE-AC02-05CH11231. The synthetic chemistry was developed under funding through the Helios Solar Energy Research Center at Lawrence Berkeley National Laboratory (LBNL). The theoretical modeling used computational facilities at the National Energy Research Scientific Computing Center (NERSC) at LBNL. EFTEM imaging was performed at the National Center for Electron Microscopy (NCEM) at LBNL. H.Z. thanks M. Watanabe, Z. Lee, and C. Song for their advice on EFTEM imaging. D.O.D. thanks W. L. Lambrecht and P. Lukashev for providing the atomic structure for high-temperature chalcocite. We thank R. Robinson for useful discussions.

Supporting Information Available: Protocols for the synthesis of the CdS nanorods and CdS−Cu_2S binary nanorods

(37) Chan, E. M.; Marcus, M. A.; Fakra, S.; ElNaggar, M.; Mathies, R. A.; Alivisatos, A. P. *J. Phys. Chem. A* **2007**, *111*, 12210–12215.
(38) Manna, L.; Wang, L. W.; Cingolani, R.; Alivisatos, A. P. *J. Phys. Chem. B* **2005**, *109*, 6183–6192.
(39) Peng, Z. A.; Peng, X. *J. Am. Chem. Soc.* **2001**, *123*, 1389–1395.
(40) Peng, X.; Wickham, J.; Alivisatos, A. P. *J. Am. Chem. Soc.* **1998**, *120*, 5343–5344.
(41) Putnis, A. *Am. Mineral.* **1977**, *62*, 107–114.

characterized in this work, a description of different phases of bulk Cu_2S, a list of the relaxed lattice constants for the CdS, Cu_2S, and Ag_2S crystals obtained in the DFT simulations, a discussion of electron counting rules for interfacial atoms in the CdS−Cu_2S interfaces, I_1 and I_2, a derivation of the individual formation energies for I_1 and I_2, and figures showing XRD simulations for the chalcocite and djurleite phases of bulk Cu_2S, the original Cd and Cu EFTEM images used to make the color composite image in Figure 3b, a schematic of the relation between monoclinic and orthorhombic cells of Cu_2S, the original supercell used to calculate the formation energy of the side attachment of Cu_2S to CdS, and auxiliary CdS structures used to determine the individual interface formation energies for I_1 and I_2. This information is available free of charge via the Internet at http://pubs.acs.org/.

JA809854Q